Zheng et al. Nanoscale Research Letters (2015) 10:293
DOI 10.1186/s11671-015-1002-4

Nanoscale Research Letters
a SpringerOpen Journal

NANO EXPRESS Open Access

In_2O_3 Nanotower Hydrogen Gas Sensors Based on Both Schottky Junction and Thermoelectronic Emission

Zhao Qiang Zheng[1,2], Lian Feng Zhu[3] and Bing Wang[1*]

Abstract

Indium oxide (In_2O_3) tower-shaped nanostructure gas sensors have been fabricated on Cr comb-shaped interdigitating electrodes with relatively narrower interspace of 1.5 μm using thermal evaporation of the mixed powders of In_2O_3 and active carbon. The Schottky contact between the In_2O_3 nanotower and the Cr comb-shaped interdigitating electrode forms the Cr/In_2O_3 nanotower Schottky diode, and the corresponding temperature-dependent *I-V* characteristics have been measured. The diode exhibits a low Schottky barrier height of 0.45 eV and ideality factor of 2.93 at room temperature. The In_2O_3 nanotower gas sensors have excellent gas-sensing characteristics to hydrogen concentration ranging from 2 to 1000 ppm at operating temperature of 120–275 °C, such as high response (83 % at 240 °C to 1000 ppm H_2), good selectivity (response to H_2, CH_4, C_2H_2, and C_3H_8), and small deviation from the ideal value of power exponent β (0.48578 at 240 °C). The sensors show fine long-term stability during exposure to 1000 ppm H_2 under operating temperature of 240 °C in 30 days. Lots of oxygen vacancies and chemisorbed oxygen ions existing in the In_2O_3 nanotowers according to the x-ray photoelectron spectroscopy (XPS) results, the change of Schottky barrier height in the Cr/In_2O_3 Schottky junction, and the thermoelectronic emission due to the contact between two In_2O_3 nanotowers mainly contribute for the H_2 sensing mechanism. The growth mechanism of the In_2O_3 nanotowers can be described to be the Vapor-Solid (VS) process.

Keywords: Nanotowers; Hydrogen; Gas sensor; Schottky junction; Thermoelectronic emission

Background

Chemical sensors based on semiconductor oxide materials have been extensively researched due to their advantageous features, such as high sensitivity, low cost, and simplicity in fabrication [1]. Among them, indium oxide (In_2O_3) semiconductive materials have been extensively studied as chemical sensors for a long time due to their advantageous features such as a wide bandgap around 3 eV, a low resistance, and good catalysis [2].

1-D In_2O_3 nanostructures show high gas-sensing response due to their high electric conductance, high transparency to visible light, strong interaction with the gas molecules, high surface-to-volume ratio, and large surface activities [3]. However, up to now, few In_2O_3 nanostructures exists good sensing properties to hydrogen. Hydrogen is the most attractive and sustainable energy for the future generations due to its high efficiency and renewable properties.

In this contribution, we report that new In_2O_3 tower-shaped nanostructures with high surface-to-volume ratio have been fabricated using thermal evaporation of the mixed powders of In_2O_3 and active carbon. The synthesized In_2O_3 nanotowers distributing on Cr comb-shaped interdigitating electrodes with relatively narrower interspace of 1.5 μm have excellent gas-sensing characteristics to hydrogen concentration ranging from 2 to 1000 ppm at operating temperature of 120–275 °C.

Methods

The fabrication of In_2O_3 nanotower hydrogen sensors includes two parts. One is the preparation of comb-shaped interdigitating electrodes with relatively narrower interspace of 1.5 μm on the silicon substrate, and the

* Correspondence: wangbing@szu.edu.cn
[1]Institute of Micro-nano Optoelectronic Technology, Shenzhen Key Lab of Micro-nano Photonic Information Technology, College of Electronic Science and Technology, Shenzhen University, Shenzhen 518060, Guangdong, People's Republic of China
Full list of author information is available at the end of the article

corresponding processes are basically the same with our previous works [4, 5].

Another part is the synthesis of In_2O_3 nanotowers on the silicon substrate by thermal evaporation of active carbon and In_2O_3 powders. The active carbon and In_2O_3 powders are mixed in a 1:1 weight ratio as the reaction source and put near the silicon substrate, which are placed inside the little quartz tube that is pulled into a large quartz tube in a horizontal tube electric furnace. After the whole system is evacuated by a vacuum pump for 20 min, the argon gas is guided into the system at 250 sccm and the pressure is kept at 350 Torr. Then, the system is rapidly heated up to 1050 °C at 40 °C/min from the room temperature and kept this temperature for 1 h. Finally, the system is cooled down to the room temperature for several hours by natural cooling. The In_2O_3 nanotowers are synthesized. Field emission scanning electron microscopy (FESEM), x-ray diffraction (XRD), and high-resolution transmission electron microscopy (HRTEM) are used to identify the morphology and structure of the products.

After that, the In_2O_3 nanotowers are scraped down from the silicon substrate and ultrasonically dispersed in ethanol for 30 min to form a suspension. Then, the suspension is taken out by straw and sprinkled on the Cr comb-shaped interdigitating electrodes so as to constitute a gas sensor chip after the ethanol evaporation. The corresponding schematic diagram of the gas sensor chip is shown in Fig. 1a. The Schottky contact between the In_2O_3 nanotower and the Cr comb-shaped interdigitating electrode forms the Schottky diode. The corresponding temperature-dependent (25–240 °C) *I-V* measurements are performed by using two regulated DC power supplies (RICH/RS1303DQ) and a digital multimeter (VICTOR/VC890D).

The heater of the gas sensor and the corresponding schematic diagram are shown in Fig. 1b, c. The heater steel silks on the thermal insulation material are connected with the metal pins "1" and "4." Each gas sensor chip is put on the heater steel silks and bonded to another two metal pins so as to constitute a sensor element. The sensor element and the corresponding schematic diagram are shown in Fig. 1d, e. When the heating voltage is applied to metal pins "1" and "4," the temperature of the heater steel silks will rise up according to Joule's law so as to make the temperature of gas sensor chip rise up. When the bias voltage is applied to metal pins "3" and "6," the electrical signal measurement for the gas sensor can be carried out. The sensor temperature at different heating voltages is measured by contacting a thermocouple to the upper side of the gas sensor chip.

Each sensor element is packaged with a stainless steel mesh cap as shown in Fig. 1f. After that, the six metal pins of each sensor element are inserted in the corresponding holes of one measurement unit in the test gas chamber as shown in Fig. 1g. There are 10 measurement units in the test gas chamber, so 10 sensor elements can be tested at the same time. Then, the test gas chamber is sealed. By controlling gas-sensing characterization system (Gyjf Technology Co. Ltd., People's Republic of China/JFO2E) consisting of gas mixer instrument, measurement instrument, and computer, certain concentration gas or air is passed into the test gas chamber based on a flow-through technique in different circumstances [6], and the corresponding schematic diagram is shown in Fig. 1h. In our case, the concentration of hydrogen gas is ranging from 2 to 1000 ppm. At the same time, bias voltage of 8.9 V is as working voltage, and certain heating voltage ranging from 3 to 5.1 V is as heating voltage which is supplied to test the gas chamber so as to apply to each tested sensor element. The resistance change of the gas sensor can be caught by the measurement instrument and displayed on the computer.

Results and Discussion

The characteristics results of the In_2O_3 nanotowers shown in Fig. 2 have been displayed in our previous work which is about the field emission properties of the In_2O_3 nanostructures [7]. The highly magnified FESEM image of the synthesized In_2O_3 nanotowers is shown in Fig. 2a. The four sides of the nanotower are chucked up with octahedrons one after another so that the nanotower posses high surface-to-volume ratio property. The corresponding XRD pattern of samples in Fig. 2b shows that the fabricated nanostructures are indexed to the cubic In_2O_3. According to PDF No. 06-0416, the lattice constants of the cubic In_2O_3 are $a = 10.118$ Å, $b = 10.118$ Å, and $c = 10.118$ Å, respectively. Figure 2c is a typical TEM bright-field image of an individual In_2O_3 nanotower with an octahedral cap size of 600 nm. The HRTEM image shown in Fig. 2d is recorded at the body section of the In_2O_3 nanotower in Fig. 2c. The interplanar spacing of 0.715 nm is corresponding to the (011) crystallographic plane of cubic In_2O_3 lattice, and the corresponding selected area electronic diffraction (SAED) pattern in Fig. 2e recorded with an electron beam perpendicular to the surface of the In_2O_3 nanotower demonstrates that the In_2O_3 nanotower is single crystal and the growth direction is along [200].

The whole synthesis is conducted under the reducing atmosphere. So, the stoichiometric proportion of In and O has been further identified by quantitative x-ray photoelectron spectroscopy (XPS) analysis (in Fig. 3) performed on the product. A wide-scan XPS spectrum shown in Fig. 3a indicated that the product is consisted mainly of In and O. The contaminated carbon is attributed to a small amount of graphite from the reaction source. For its XPS spectrum of In 3d shown in Fig. 3b, because of the spin-

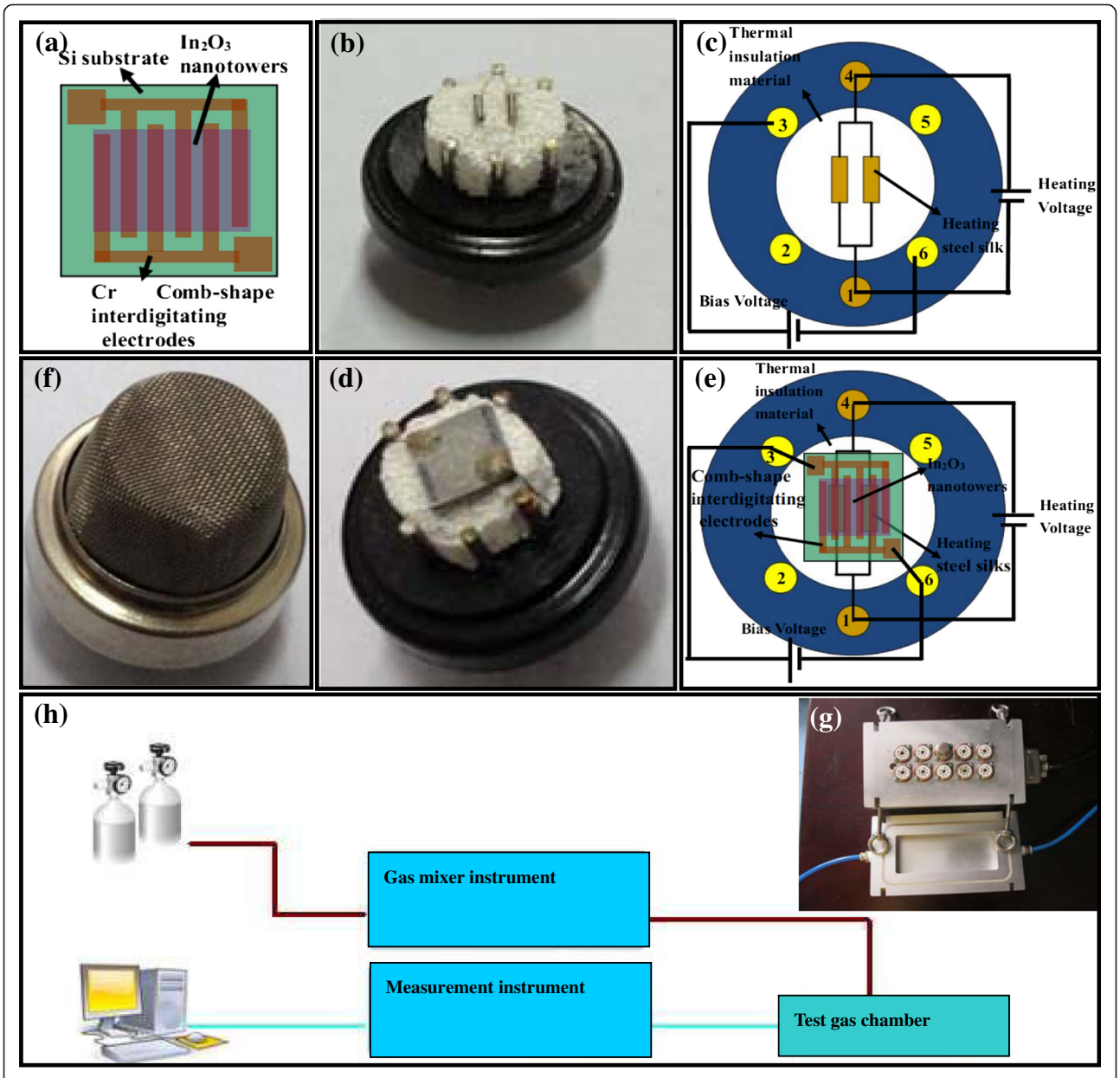

Fig. 1 **a** The schematic diagram of the gas sensor chip. **b**, **c** The heater of the gas sensor and the corresponding schematic diagram. **d**, **e** The sensor element and the corresponding schematic diagram. **f** The sensor element packaged with a stainless steel mesh cap. **g** The test gas chamber. **h** The schematic diagram of the gas-sensing characterization system

orbital splits, In $3d_{5/2}$ and In $3d_{3/2}$ have characteristic double peaks located at 444.96 and 453 eV, respectively, corresponding to the binding energy of In^{3+} in In_2O_3 [8]. For its XPS spectrum of O1s shown in Fig. 3c, the O1s peaks can be divided into two peaks, centered at 530 eV (OI) and 532 eV (OII), respectively. The OI sub peak is assigned to the lattice oxygen in the In_2O_3 nanotower [8–11], and the OII sub peak is usually associated with the chemisorbed oxygen ions in the oxygen vacancy (V_o) region [8, 10, 11]. The atomic ratio of O:In was 4.4:1, which did not agree with the stoichiometric proportion of O and In presenting in In_2O_3. Excrescent O may be adsorption oxygen [12]. As the area ratio of OI/OII is about 1/4.6, so the chemical formula of the nanotowers is $In_2O_{1.57}$, implying that a large amount of oxygen vacancies are introduced in the product.

Temperature-dependent *I-V* plots for representative Cr/In_2O_3 nanotower Schottky diode before exposure to H_2 are shown in Fig. 4a. The primary conduction mechanism at Schottky diodes, in general, is due to the flow of majority charge carriers over the barrier by a thermionic process [13]. The electrical characterization of a

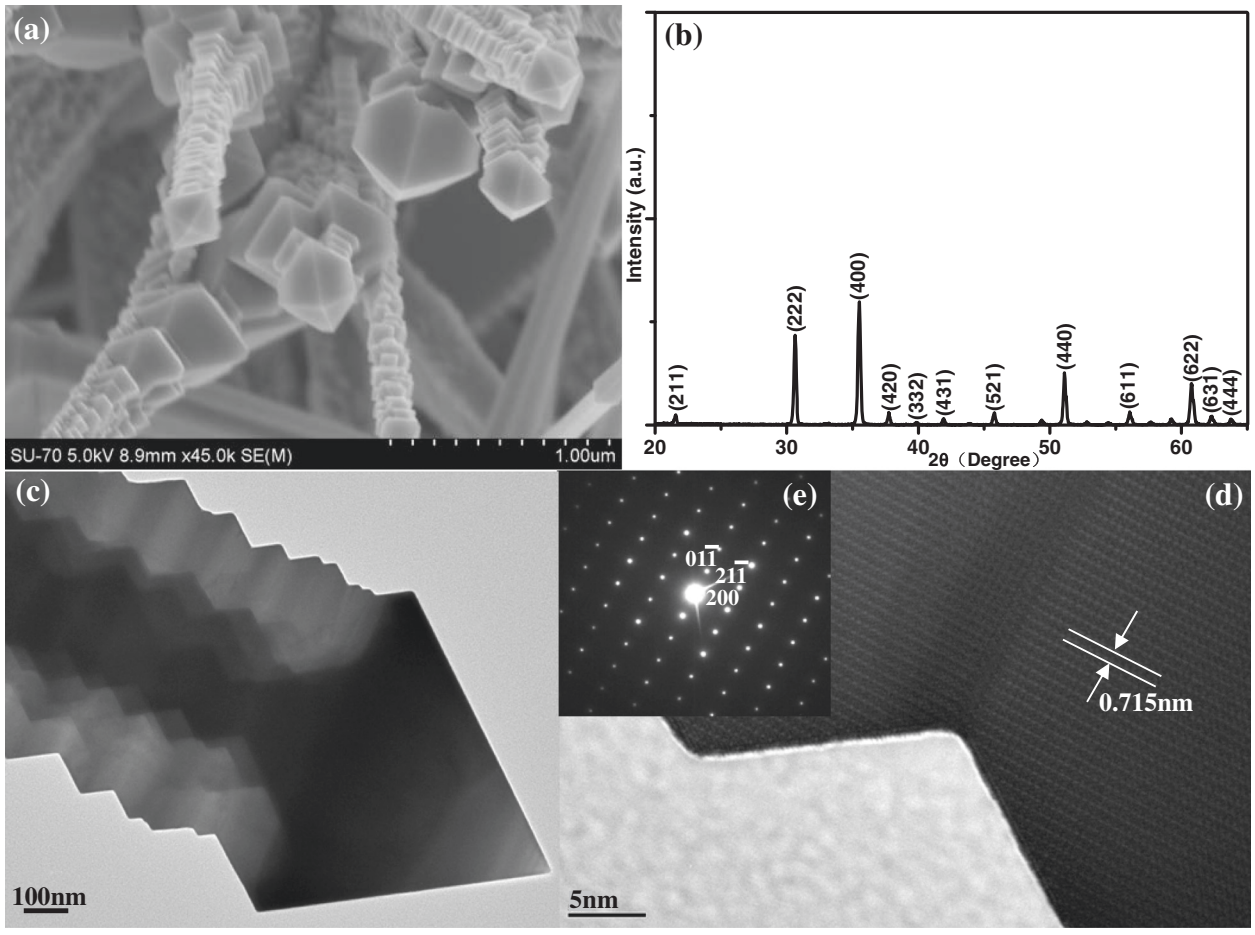

Fig. 2 **a** The highly magnified FESEM image and **b** the XRD pattern of the In_2O_3 nanotowers [7]. **c** The bright-field image, **d** the HRTEM image, and **e** the SAED pattern of an individual In_2O_3 nanotower [7]

Schottky diode necessitates the determination of the barrier height and the ideality factor. For an ideal diode, the diode ideality factor should be nearly equal to unity. But in a real situation, it may increase when the effects of series resistance, leakage current, etc. come into play [13]. Depending on the temperature (T) and applied voltage (V), different transport mechanisms might be simultaneously operative in the Schottky diode and modulate the charge transport. Assuming that the thermionic emission is the most predominant mechanism, the general form of the temperature dependence of the current may be expressed as [13–15]:

$$I = AA^* \exp(-\beta\phi_B) \exp\left[\frac{\beta(V-IR)}{n}\right] \quad (1)$$

where, ϕ_B is the effective barrier height, A is the junction area, A^* is the Richardson constant, n is the ideality factor, R is the series resistance, and $\beta = q/kT$. In such a case, the generalized Norde method can be used to evaluate the effective barrier height and diode ideality factor from I-V measurements [13, 14]. The effective barrier height and ideality factor measured at different temperatures for Cr/In_2O_3 nanotower Schottky diode are shown in Fig. 4b. The barrier height can be seen to increase linearly with temperature. On the other hand, the ideality factor for the Schottky diode decreases from 2.93 to 0.82 with an increase in temperature. Deviation of the ideality factor from unity may be due to the existence of high series resistance [14].

H_2 sensing characteristics are investigated when the sensor are exposed to different H_2 concentrations ranging from 2 to 1000 ppm. The different heating voltages of 3, 3.5, 4, 4.5, and 5.1 V correspond to the different substrate temperatures of 120, 160, 200, 240, and 275 °C, respectively. The measurement time is 3500 s in the whole test process. Sensor resistances decrease abruptly upon exposure to H_2 and recover to initial values after purging by dry air. After several circles between the test gas and dry air, the In_2O_3 nanotowers sensor can still recover to the initial states, indicating good reversibility. The responses of the sensor are shown in Fig. 5a. We calculated

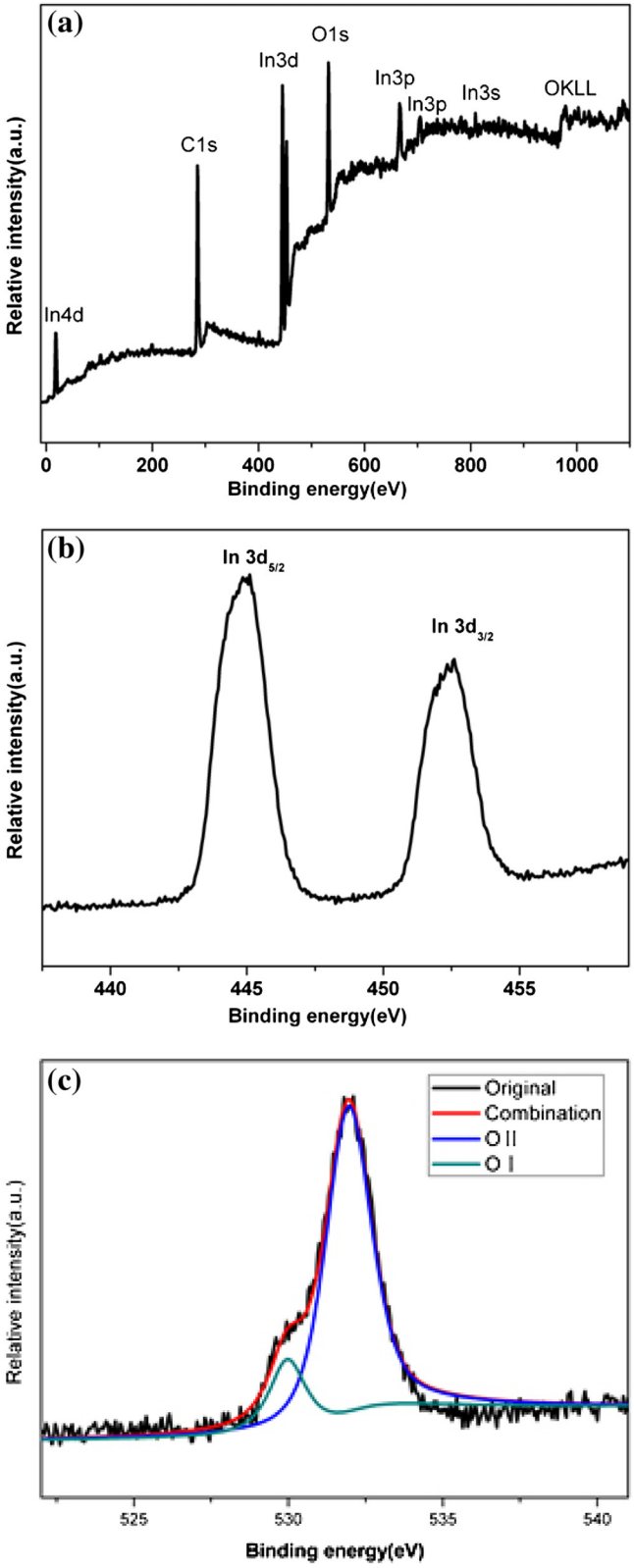

Fig. 3 **a** Wide-scan XPS spectrum of the In_2O_3 nanotowers. **b** Its spectrum of In 3d. **c** Its spectrum of O1s

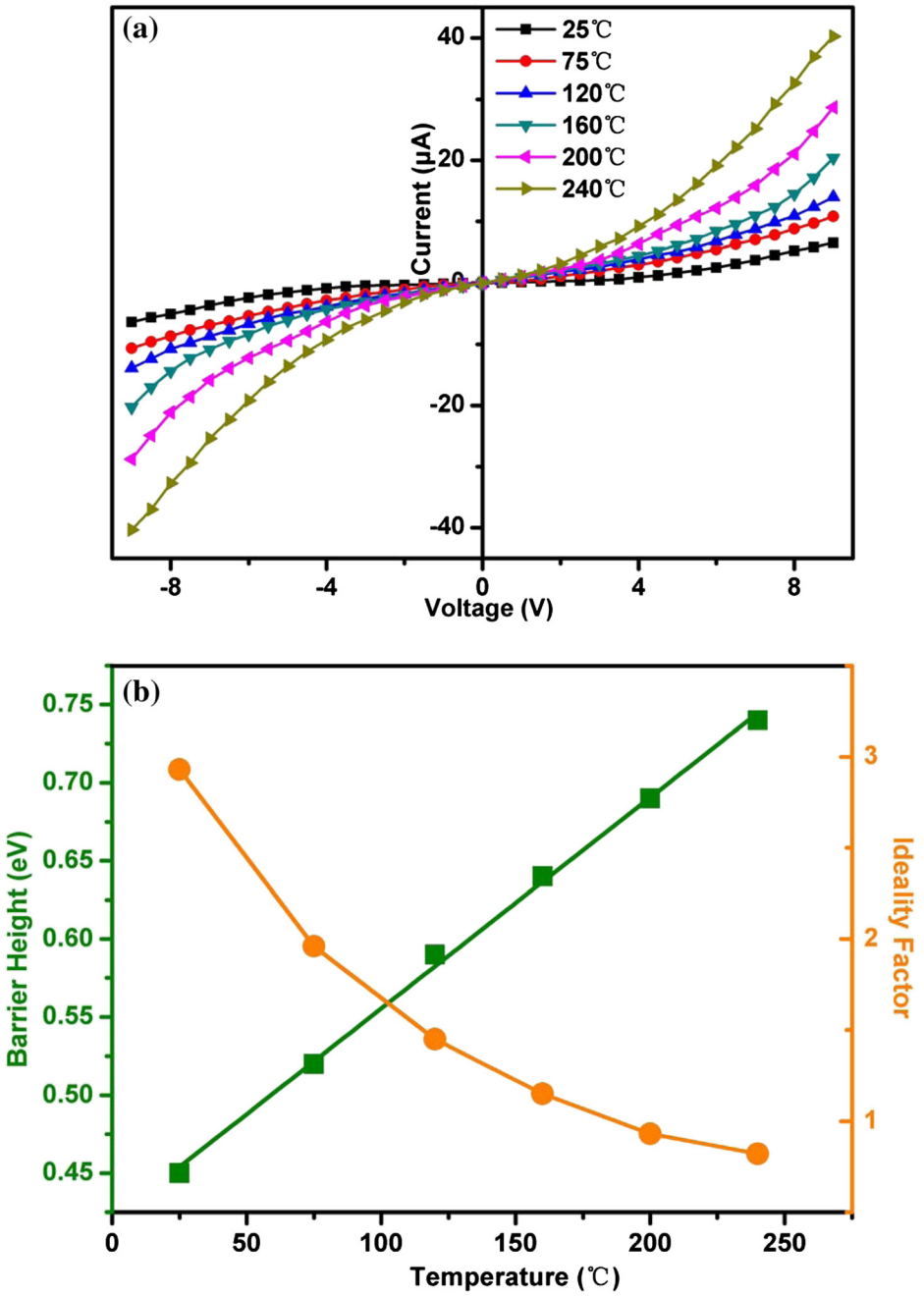

Fig. 4 a Temperature-dependent *I-V* characteristics for representative Cr/In_2O_3 nanotower Schottky diode before H_2 exposure. **b** Variation of barrier height (φ_B) and ideality factor (n) with temperature for Cr/In_2O_3 nanotower Schottky diode

the response of the sensor using the expression of Response% = $(R_o - R_g)/R_o$*100 % [16]. Here, R_o and R_g are the resistance of the sensor before and after exposure to the tested gas, respectively. Figure 5b shows the response as a function of operating temperatures from 120 to 275 °C for the sensor exposed to different H_2 concentrations of 2–1000 ppm. In_2O_3 nanotower gas sensor reaches the maximum response value of 83 % at an optimal operating temperature of 240 °C.

During exposure to increasing H_2 concentrations ranging from 2 to 1000 ppm under the optimal operating temperature of 240 °C, the steady-state resistance response of the sensor is also investigated and shown in Fig. 6a. According to the Zhu et al. [16], this should be done in a stable environment, and the time of measurement should be longer enough to insure adsorption of hydrogen molecules to reach a steady state. Figure 6b shows that the corresponding steady-state conductance

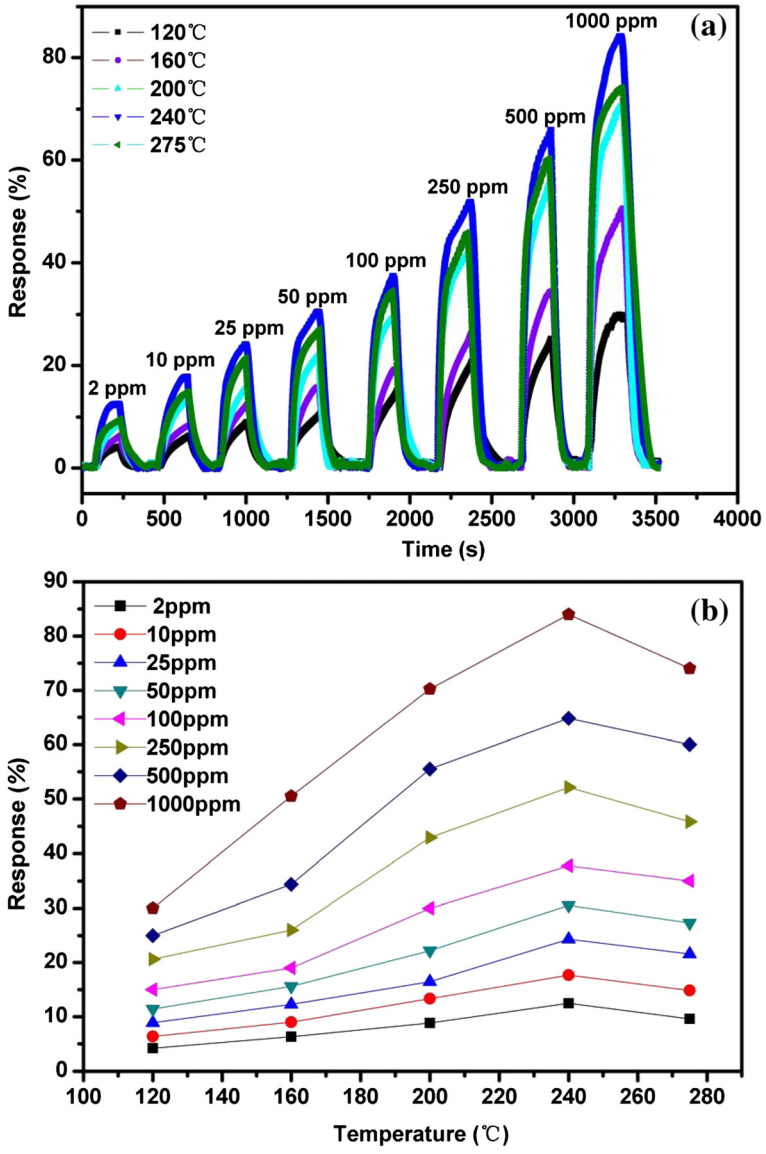

Fig. 5 a Typical response curves and **b** the response as a function of operating temperature of In_2O_3 nanotower gas sensor exposed to H_2 concentrations ranging from 2 to 1000 ppm and tested at 120–270 °C, respectively

($G = 1/R$) of the sensor follows a power law depending on the H_2 gas concentration, $G_{gas} = G_{air} + \alpha(\text{concentration})^{\beta}$, where α is a constant, β is a power exponent, and the ideal value is 0.5 [17]. The experimental data deduced from the measurement results in Fig. 6a is well consistent with the exponent fitting results, and the corresponding values of α, β, and correlation coefficient R obtained in the process of fitting are indicated in Fig. 6b. For the β value of 0.48578, the small deviations from the ideal value of 0.5 probably relate to either agglomeration or zones in the structure that are less sensitive to H_2 than others, as modeled by Scott et al. [18].

Response time is also an important parameter for a gas sensor, which is defined here as the time reaching 90 % of the final equilibrium value [19]. The corresponding response time of the sensor exposed to H_2 concentrations of 2–1000 ppm at the operating temperature of 240 °C is indicated in Fig. 7a. With the hydrogen concentration increasing from 2 to 1000 ppm, the response time decreases from 127 to 63 s. To be sure, although interdigitating gap is smaller, the response time is relatively longer compared with that of the relevant report [20]. As for the reasons, we would like to elaborate on two aspects. Firstly, it is related with the longer path between the gas mixer instrument and the test gas chamber as shown in Fig. 1h. Secondly, the relatively larger size of our nanotowers compared with that of relevant report [20] results in a correspondingly less

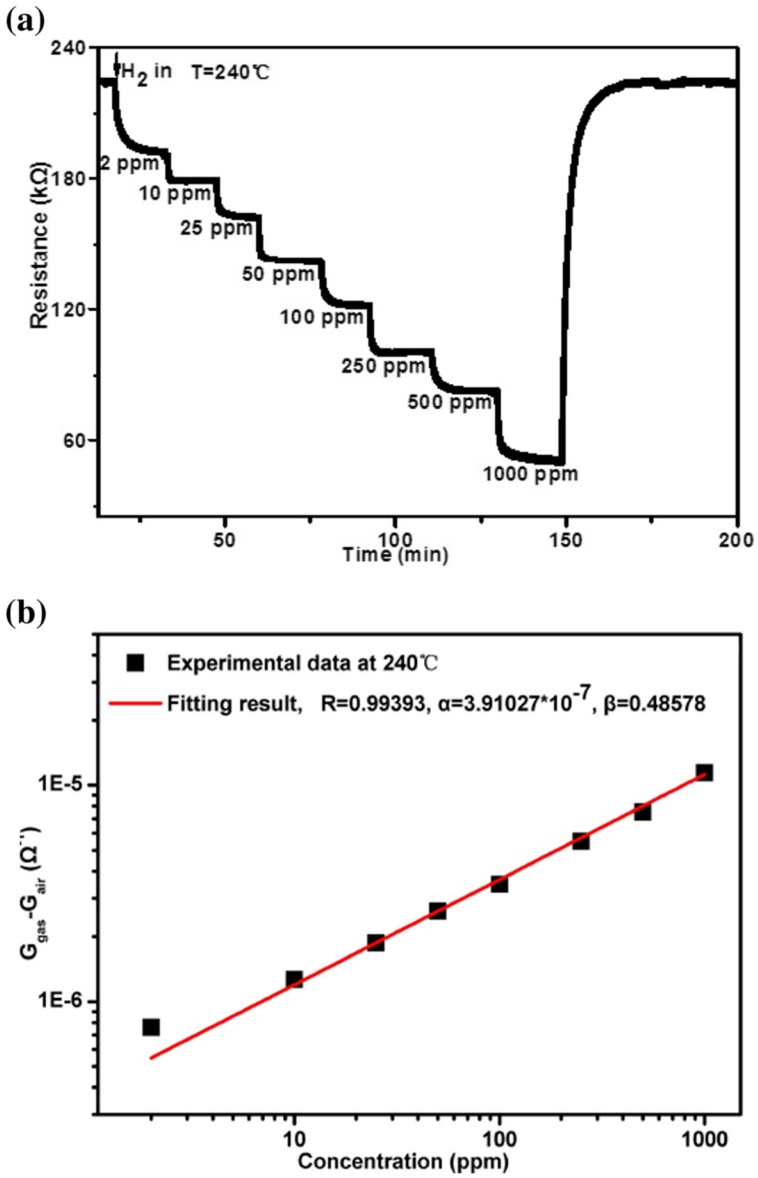

Fig. 6 a The steady-state resistance responses of the sensor during exposure to increasing H_2 concentrations (between 2 and 1000 ppm) under an optimal operating temperature of 240 °C. **b** The corresponding steady-state conductance of the sensor as a function of the H_2 concentration

surface-to-volume ratio, which can increase the response time too [20–22]. The time dependence of resistance of the In_2O_3 nanotowers on exposure to 500 ppm H_2 at different operating temperatures of 120–240 °C is shown in Fig. 7b. The rate of resistance change becomes greater as the temperature increases. The inset figure shows the rate of Arrhenius plot for the resistance change of nanostructures. An adsorption activation energy of 24.67 kJ/mol for the In_2O_3 nanotowers as shown in Fig. 7b is larger than that of 11.8 kJ/mol for the Pd-coated ZnO nanowires [23], that of 2.2 kcal/mol for the Pd-coated GaN nanowires [24], and that of 23.6 kJ/mol for the Pt-coated $W_{18}O_{49}$ nanowire networks [16].

Selectivity of the gas sensor is very important in the gas-sensing application. As we know, In_2O_3 is one kind of broad-spectrum sensitive material. The selective property is tested by exposing the sensor in reducing gases such as CH_4, C_3H_8, C_2H_2, CO, C_2H_5OH, and H_2, respectively, which is shown in Fig. 8a. The concentration values are 10, 100, and 1000 ppm, and the operating temperatures are 120 and 240 °C. It is very clear to discover that the sensor exhibits much higher responses to H_2 in comparison to that of CH_4, C_3H_8, and C_2H_2, respectively, which is due to the reason that the hydrogen with the smallest molecular size can easily pass through the surface dense layer and react intensely with the negatively charged

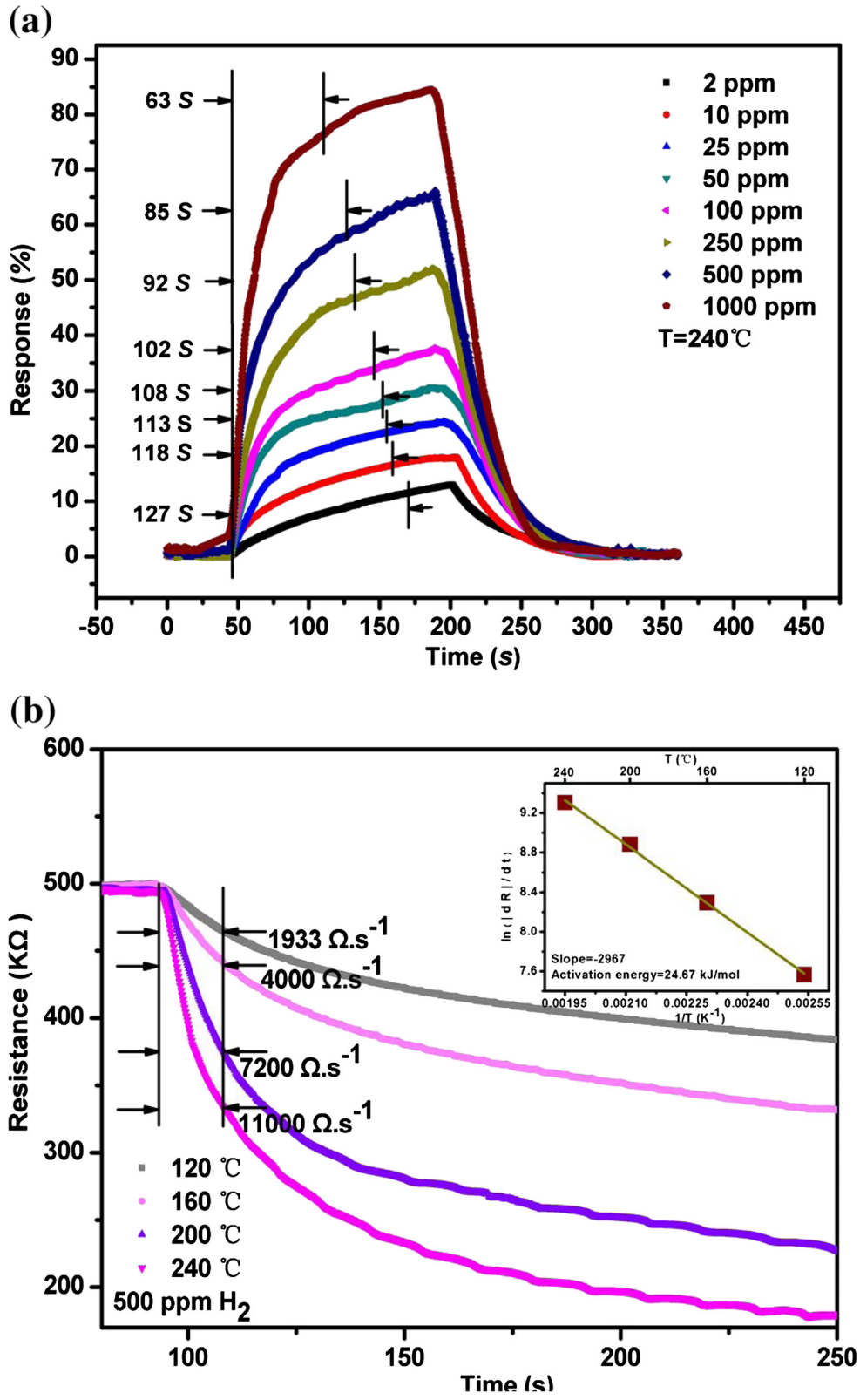

Fig. 7 a One cycle of H_2 in and out in the concentration range of 2–1000 ppm under an optimal operating temperature of 240 °C for the sensor. **b** Resistance vs. time on exposure to 500 ppm of H_2 under different operating temperatures of 120–240 °C from the sensor, the *inset figures* showing the corresponding Arrhenius plot based on the rates of change of the resistance

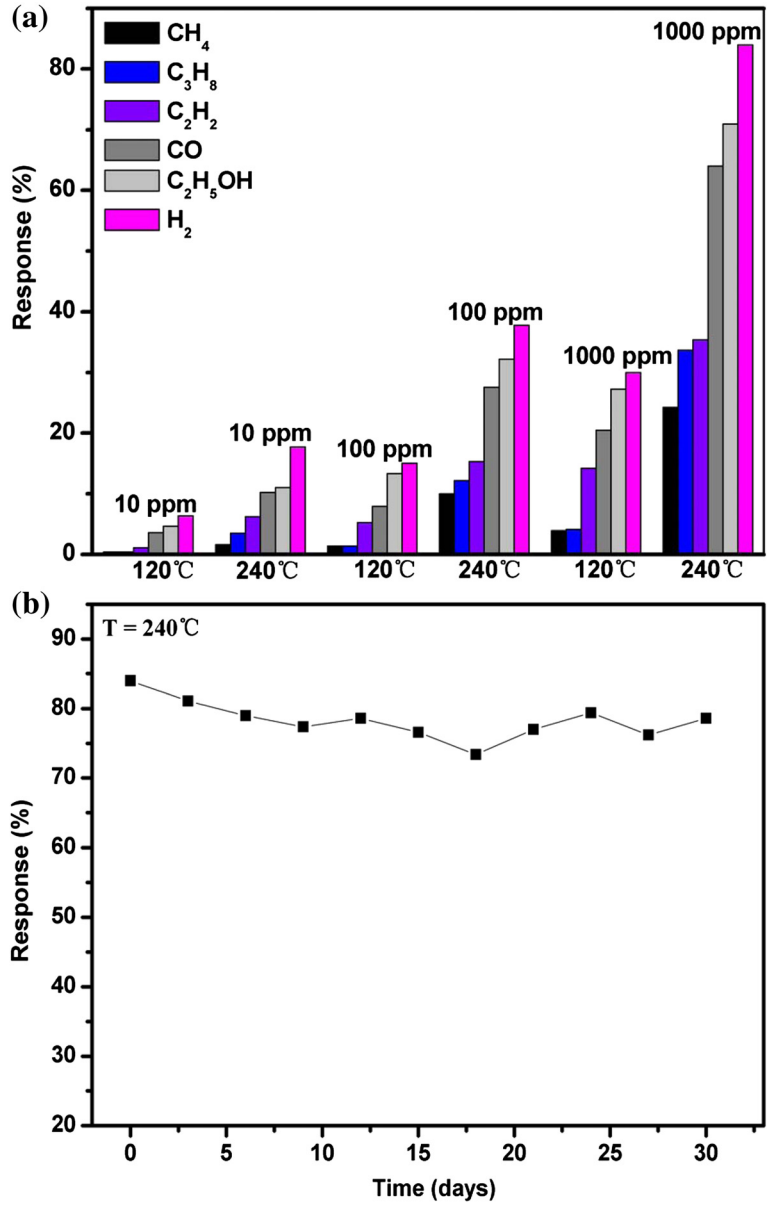

Fig. 8 a The selectivity properties of the sensor to reducing gases such as CH_4, C_3H_8, C_2H_2, CO, C_2H_5OH, and H_2, at the concentration of 10, 100, and 1000 ppm and under the different operating temperatures of 120 and 240 °C. **b** Long-term stability of the sensor to 1000 ppm H_2 at the operating temperature of 240 °C in 30 days

oxygen adsorbates on the In_2O_3 surface [20]. However, the sensor exhibits slightly higher responses to H_2 than that of CO and C_2H_5OH, respectively, which is largely related with the activation energy of CO and C_2H_5OH being close to hydrogen. So, further study should be focused on improving the selectivity of the In_2O_3 nanotower gas sensors through surface modification with noble metals (Pt, Pd, Au, etc.). In addition, temperature modulation is also another efficient method for improving the selectivity of the metal oxide gas sensors [25]. Moreover, in order to improve the selectivity of the sensor to the macromolecular gas such as CO or C_2H_5OH, we take an effective method to install the activated carbon or zeolites on the cover of the sensors.

The long-term stability of the sensor is also displayed in Fig. 8b. We measure the response of the sensor to 1000 ppm H_2 at an operating temperature of 240 °C every 3 days. Clearly, the sensor shows relatively stable response in 30 days.

Hydrogen-sensing response of the In_2O_3 nanotower gas sensor operated at 240 °C in comparison to those of the reported sensors using In_2O_3-based nano- or micro-

structured materials is shown in Table 1. The range of the Response% of all the sensors normalized to $(R_o - R_g)/R_o$*100 % is from 0 to 100 % due to R_g smaller than R_o and greater than 0. Thus, these results definitely show that the In_2O_3 nanotower hydrogen sensor has basically achieved better responses than those of the reported sensors [3, 26–38].

The growth mechanism of the In_2O_3 nanotowers can be described to be the VS process, and the corresponding schematic illustration is shown in Fig. 9a. It is well-known that the growth rate perpendicular to different planes is proportional to their surface energies. For In_2O_3 with a bcc structure, the surface energy relationships among three low-index crystallographic planes should correspond to $\gamma\{111\} < \gamma\{100\} < \gamma\{110\}$ [39]. The shape of the pyramid tip is consistent with the cubic crystal structure of In_2O_3 [40]. In the In_2O_3 cubic structure, the {001} family planes contain the three equivalent planes (100), (010), and (001), which are perpendicular to the three directions [100], [010], and [001], respectively. Pyramids bounded by {111} facets with the highest (111) to that of (100) surface energy ratio possess the lowest surface energy [40]. The difference of surface energies among {110}, {100}, and {111} facets can lead to their different growth rates, and the growth rates of three growth directions have such relationships: $r_{[111]} < r_{[100]} < r_{[110]}$ [39]. As shown in the inset figure in Fig. 9a, after the 0-D growth, the (110) plane will disappear earlier, and the (111) plane will be preserved [39]. At the initial stage of heating, the indium vapor gradually evaporates out of the In oxide through a carbothermal reduction reaction, so the saturation ratio is low at this stage. Under a low saturation ratio, the 0-D nucleation and growth begin, and an octahedron forms under a VS mechanism [39], which is shown in the first process. According to a self-catalyzed effect, the surface polarity of the (111) plane of the cubic lattice in In_2O_3 octahedron can depress the relatively high nucleation potential barrier of In_2O_3 at the low temperature and induce the In_2O_3 nucleation on the plane [41]. Therefore, the four little 0-D In_2O_3 octahedrons can be formed at the four (111) plane of the big In_2O_3 octahedron, which is shown in the second process. During the 0-D growth, the indium vapor is uninterruptedly evaporated, so the saturation ratio gradually increases and finally reaches the critical value of the 1-D growth. Then, the 1-D growth at the top plane of the four little 0-D In_2O_3 octahedrons along the [200] direction begins. The 1-D growth consumes abundant reagent species and results in a decrease in the saturation ratio, so the 1-D growth stops and new 0-D growth begins. The 0-D growth will make the newly formed four little octahedral configurations. During the 0-D growth, the saturation ratio increases, and a new round of 1-D growth begins [39]. After the alternating 0-D and 1-D growths, the body of tower-shaped nanostructure continuously grows out, which is shown in the third process. As the reaction between the In_2O_3 powders and the active carbon from the initial stage develops, the reagent's vapor pressure turns bigger and bigger. The continuously increasing

Table 1 Hydrogen-sensing response of the In_2O_3 nanotowers sensor operated at 240 °C in comparison to those of the reported sensors using In_2O_3-based nano- or micro-structured materials

Type	Operated temperature (°C)	Response% ($\Delta R/R_o$*100 %) toward H_2 under the following concentrations (ppm)						
		2	10–50	150–270	400–500	1000	2000	4000
In_2O_3 nanotowers	240	13	21	50	64	83		
In_2O_3 nanowires [3]	400			17	60			
In_2O_3 nanoneedles [3]	350			10.7	20			
ZnO/In_2O_3 nanorods [26]	20–25		9.8	15.5	20.5			
In_2O_3 thin films [27]	50				6.5			
In_2O_3 nanowires [28]	200				10			
Au-loaded In_2O_3 nanofibers [29]	140				33			
In_2O_3 hollow nanospheres [30]	300			41				
In_2O_3 nanowires [31]	300						69	
In_2O_3/ZnO nanowires [32]	400						83	
In_2O_3 nanowires [32]	300							71
In_2O_3 flower-like microspheres [33]	150					10		
In_2O_3 urchin-like microspheres [34]	150					10		
In_2O_3/La/Pd [35]	100				3			
In_2O_3 nanofibers [36]	300			43				
In_2O_3 nanowires [37]	250					17.9		
In_2O_3:Se [38]	–					40		

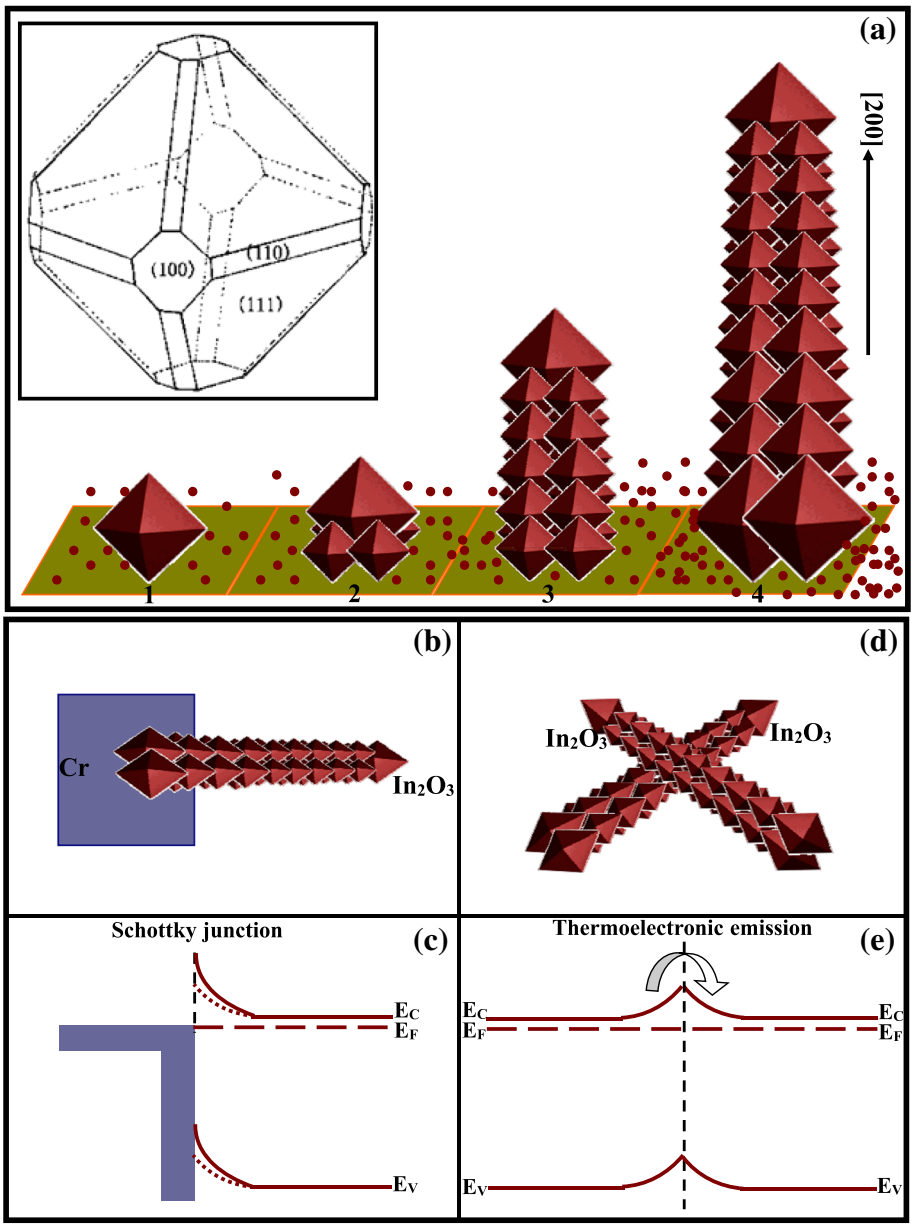

Fig. 9 a The growth mechanism of the In_2O_3 nanotower, the *inset figure* is the schematic illustration of 0-D growth with octahedral configuration under the VS mechanism [39]. **b** The Cr/In_2O_3 Schottky junction and **c** the corresponding energy-level diagram. **d** The contact between two In_2O_3 nanotowers and **e** the corresponding energy-level diagram

reagent's vapor pressure will continuously lead to large lateral and small axial growth rates, which will induce to the formation of 1-D structure with continuously increased size [42]. Therefore, the size of the In_2O_3 nanotowers can be continuously increased from top to bottom as shown in the fourth process.

The unique hydrogen-sensing properties based on the In_2O_3 nanotower can be explained as follows. In the open air, the chemisorbed oxygen ions (O_2^- or O^-) form on the surface of the In_2O_3 nanotowers leading to a depletion region in surface layer owing to the electron shift from In_2O_3 to oxygen. When the hydrogen is injected, H_2 reacts with chemisorbed oxygen ions, which releases electrons back to the surface of the In_2O_3 nanotowers and alter its electrical conductivity of the structures. According to the XPS spectrum of O1s shown in Fig. 3c, it appears that a high concentration of chemisorbed oxygen ions will favor the forward reaction [2]. For example, it is found that the ethanol-sensing responses of In_2O_3 increase with the increasing intensity of chemisorbed oxygen [9]. In addition, because of the response of the metal oxide sensor to methanol depending on

the basicity of the metal oxide [43] and the basicity controlled by the electronic density which is generated from the V_o [9], the hydrogen-sensing properties of the In_2O_3 nanotowers are excellent due to lots of V_o being introduced in the In_2O_3 nanotowers in this paper.

The hydrogen-sensing mechanism of the sensors is attributed to not only the hydrogen-sensing properties based on the In_2O_3 nanotower discussed above but also the structure characteristics of the sensors as schematically shown in Fig. 9b–e. Besides the change of the Schottky barrier height in the Cr/In_2O_3 Schottky junction as shown in Fig. 9b, c, the thermoelectronic emission due to the contact between two In_2O_3 nanotowers as shown in Fig. 9d, e will contribute for the hydrogen-sensing mechanism too.

The electrical response comes from the variation of the Schottky barrier height and barrier width as a result of adsorption of gaseous species at the Schottky contact. The response due to adsorption can be explained from the band diagram at the metal/nanostructure contact. After the exposure to H_2, Cr adsorbs H_2 by catalytic chemical adsorption, which reduces the Schottky barrier height [14]. The catalytic effect of chromium can be understood in two ways [44]. The first one is related to the work function value of the chromium which leads to an excess of free bonds near the surface region, then producing an important oxidation which favors the subsequent reactions with the H_2. The second one is related to the formation of a Cr_2O_3 phase close to the surface region, which increases the catalytic activity of this region due to the fact that the surface chromium atoms can be easily oxidized and reach an effective valence of four. So, they can adsorb a complete monolayer of active oxygen.

In an individual In_2O_3 nanotower, free carriers (electrons) can transport along the conduction channel. But when transporting between two contacting In_2O_3 nanotowers, the electrons have to pass through a potential barrier at the junctions and a thermoelectronic emission mechanism can be used to describe the electron transportation in the junctions [16]. The change in resistance during the adsorption or desorption process of H_2 species is likely to be caused by the alteration both in the width of the surface depletion layer of each In_2O_3 nanotower and in the height of potential barriers built at the contacted junctions between two In_2O_3 nanotowers. These two-fold effects may facilitate less response time and higher response to certain chemical species [45].

Conclusions

In summary, we report that new In_2O_3 nanotowers synthesized via thermal evaporation and distributed on Cr comb-shaped interdigitating electrodes with relatively narrower interspace of 1.5 μm have high response, fine long-term stability, and small deviation from ideal value of power exponent β, in the hydrogen concentration ranging from 2 to 1000 ppm and at the operating temperature of 120–275 °C. The Schottky contact between the In_2O_3 nanotower and the Cr comb-shaped interdigitating electrode forms the Cr/In_2O_3 nanotower Schottky diode, and the corresponding temperature-dependent I-V characteristics have been measured. The diode exhibits a low Schottky barrier height of 0.45 eV and ideality factor of 2.93 at room temperature. The growth mechanism of the In_2O_3 nanotowers has been discussed in detail, which is account for the high surface-to-volume ratio of the morphology. Lots of oxygen vacancies and chemisorbed oxygen ions exist in the In_2O_3 nanotowers according to the XPS results. The change of Schottky barrier height in the Cr/In_2O_3 Schottky junction and the thermoelectronic emission due to the contact between two In_2O_3 nanotowers mainly contribute for the H_2 sensing mechanism. The In_2O_3 nanotowers hydrogen sensors are promising for further practical applications.

Competing Interests

The authors declare that they have no competing interests.

Authors' Contributions

ZQZ carried out all the experimental processes, characterization, and mechanism research. LFZ conceived the study and participated in its coordination. BW drafted the manuscript. All authors read and approved the final manuscript.

Acknowledgements

This work was supported by National Natural Science Foundation of China (50902097), Basic Research Project of Shenzhen (JCYJ20140418193546110), Guangdong Natural Science Foundation of China (9451806001002303), Project of the Department of Education of Guangdong Province (2013KJCX0165), Outstanding Young Teacher Training Project in the institutions of higher learning of Guangdong Province (Yq2013145), and Open Project of Shenzhen Key Laboratory of Micro-nano Photonic Information Technology (MN201405).

Author details

[1]Institute of Micro-nano Optoelectronic Technology, Shenzhen Key Lab of Micro-nano Photonic Information Technology, College of Electronic Science and Technology, Shenzhen University, Shenzhen 518060, Guangdong, People's Republic of China. [2]State Key Laboratory of Optoelectronic Materials and Technologies, Nanotechnology Research Center, School of Physics & Engineering, Sun Yat-sen University, Guangzhou 510275Guangdong, People's Republic of China. [3]Department of Materials Science and Engineering, Tsinghua University, Beijing 100084, People's Republic of China.

Received: 16 March 2015 Accepted: 5 July 2015
Published online: 15 July 2015

References

1. Zeng ZM, Wang K, Zhang ZX, Chen JJ, Zhou WL. The detection of H_2S at room temperature by using individual indium oxide nanowire transistors. Nanotechnology. 2009;20:045503.
2. Xu JQ, Wang XH, Shen JN. Hydrothermal synthesis of In_2O_3 for detecting H_2S in air. Sens Actu B. 2006;115:642.
3. Qurashi A, El-Maghraby EM, Yamazaki T, Kikuta T. Catalyst supported growth of In_2O_3 nanostructures and their hydrogen gas sensing properties. Sens Actu B. 2010;147:48.
4. Wang B, Zhu LF, Yang YH, Xu NS, Yang GW. Fabrication of a SnO_2 nanowire gas sensor and sensor performance for hydrogen. J Phys Chem C. 2008;112:6643.

5. Wang B, Zheng ZQ, Zhu LF, Wu HY, Yang YH. Self-assembled and Pd decorated Zn_2SnO_4/ZnO wire-sheet shape nano-heterostructures networks hydrogen gas sensors. Sens Actu B. 2014;195:549.
6. Hwang IS, Kim SJ, Choi JK, Jung JJ, Yoo DJ, Dong KY, et al. Large-scale fabrication of highly sensitive SnO_2 nanowire network gas sensors by single step vapor phase growth. Sens Actu B. 2012;165:97.
7. Wang B, Zheng ZQ, Wu HY, Zhu LF. Field emission properties and growth mechanism of In_2O_3 nanostructures. Nano Res Lett. 2014;9:111.
8. Du JM, Huang L, Chen ZQ. A controlled method to synthesize hybrid In_2O_3/Ag nanochains and nanoparticles: surface-enhanced Raman scattering. J Phys Chem C. 2009;113:9998.
9. Gu FB, Zhang L, Wang ZH, Han DM, Guo GS. Fine-tuning the structure of cubic indium oxide and their ethanol-sensing properties. Sens Actu B. 2014;193:669.
10. Wang SQ, An YK, Feng DQ, Wu ZH, Liu JW. The local structure, magnetic, and transport properties of Cr-doped In_2O_3 films. J Appl Phys. 2013;113:153901.
11. Yan SM, Ge SH, Zuo YL, Qiao W, Zhang L. Room-temperature ferromagnetism in Er-doped ZnO thin films. Scr Mater. 2009;61:387.
12. Wu XC, Hong JM, Han ZJ, Tao YR. Fabrication and photoluminescence characteristics of single crystalline InO nanowires. Chem Phys Lett. 2003;373:28–32.
13. Das SN, Pal AK. Hydrogen sensor based on thin film nanocrystalline n-GaN/Pd Schottky diode. J Phys D App Phys. 2007;40:7291.
14. Das SN, Kar JP, Choi JH, Lee TI, Moon KJ, Myoung JM. Fabrication and characterization of ZnO single nanowire-based hydrogen sensor. J Phys Chem C. 2010;114:1689.
15. Sze SM. Physics of semiconductor devices. New York: Wiley; 1979.
16. Zhu LF, She JC, Luo JY, Deng SZ, Chen J, Ji XW, et al. Self-heated hydrogen gas sensors based on Pt-coated $W_{18}O_{49}$ nanowire networks with high sensitivity, good selectivity and low power consumption. Sens Actu B. 2011;153:354.
17. Kim I, Rothschild A, Hyodo T, Tuller HL. Microsphere templating as means of enhancing surface activity and gas sensitivity of $CaCu_3Ti_4O_{12}$ thin films. Nano Lett. 2006;6:193.
18. Scott RWJ, Yang SM, Chabanis G, Coombs N, Willams DE, Ozin GA. Tin dioxide opals and inverted opals: near-ideal microstructures for gas sensors. Adv Mater. 2001;13:1468.
19. Li J, Fan HQ, Jia XH. Multilayered ZnO nanosheets with 3D porous architectures: synthesis and gas sensing application. J Phys Chem C. 2010;114:14684.
20. Ahsanulhaq Q, Toshinari Y, Maghraby EME, Toshio K. Fabrication and gas sensing properties of In_2O_3 nanopushpins. Appl Phys Lett. 2009;95:153109.
21. Wei SH, Wang SM, Zhang Y, Zhou MH. Different morphologies of ZnO and their ethanol sensing property. Sens Actu B. 2014;192:480.
22. Huang BR, Lin JC. A facile synthesis of ZnO nanotubes and their hydrogen sensing properties. Appl Surf Sci. 2013;280:945.
23. Wang HT, Kang BS, Ren F, Tien LC, Sadik PW. Hydrogen-selective sensing at room temperature with ZnO nanorods. Appl Phys Lett. 2005;86:243503.
24. Lim W, Wright JS, Gila BP, Johnson J, Ural A, Anderson T, et al. Room temperature hydrogen detection using Pd-coated GaN nanowires. Appl Phys Lett. 2008;93:072109.
25. Huang JR, Gu CP, Meng FL, Li MQ, Liu JH. Detection of volatile organic compounds by using a single temperature-modulated SnO_2 gas sensor and artificial neural network. Smar Mater Stru. 2007;16:701.
26. Huang BR, Lin JC. Core-shell structure of zinc oxide/indium oxide nanorod based hydrogen sensors. Sens Actu B. 2012;174:389.
27. Bari RH, Ppatil P, Patil SB, Bari A. Detection of H_2S gas at lower operating temperature using sprayed nanostructured In_2O_3 thin films. Bull Mater Sci. 2013;36:967.
28. Chen PC, Ishikawa F, Chang HK, Ryu KM, Zhou CW. Ananoelectronic nose: a hybrid nanowire/carbon nanotube sensor array with integrated micromachined hotplates for sensitive gas discrimination. Nanotechnology. 2009;20:125503.
29. Xu XJ, Fan HT, Liu YT, Wang LJ, Zhang T. Au-loaded In_2O_3 nanofibers-based ethanol micro gas sensor with low power consumption. Sens Actu B. 2011;160:713.
30. Kim SJ, Hwang IS, Choi JK, Kang YC, Lee JH. Enhanced C_2H_5OH sensing characteristics of nano-porous In_2O_3 hollow spheres prepared by sucrose-mediated hydrothermal reaction. Sens Actu B. 2011;155:512.
31. Singh ND, Ponzoni A, Gupta RK, Lee PS, Comini E. Synthesis of In_2O_3-ZnO core-shell nanowires and their application in gas sensing. Sens Actu B. 2011;160:1346.
32. Singh ND, Ponzoni A, Comini E, Lee PS. Chemical sensing investigations on Zn–In_2O_3 nanowires. Sens Actu B. 2012;171:244.
33. Xu XM, Zhao PL, Wang DW, Sun P, You L, Sun YF, et al. Preparation and gas sensing properties of hierarchical flower-like In_2O_3 microspheres. Sens Actu B. 2013;176:405.
34. Xu XM, Mei XD, Zhao PL, Sun P, Sun YF, Hu XL, et al. One-step synthesis and gas sensing characteristics of urchin-like In_2O_3. Sens Actu B. 2013;186:61.
35. Kapse VD, Ghosh SA, Raghuwanshi FC, Kapse SD. Enhanced H_2S sensing characteristics of La-doped In_2O_3: effect of Pd sensitization. Sens Actu B. 2009;137:681.
36. Zheng W, Lu XF, Wang W, Li ZY, Zhang HG, Wang Y, et al. A highly sensitive and fast-responding sensor based on electrospun In_2O_3 nanofibers. Sens Actu B. 2009;142:61.
37. Qurashi A, El-Maghraby EM, Yamazaki T, Shen YB, Kikuta T. A generic approach for controlled synthesis of In_2O_3 nanostructures for gas sensing applications. J All Comp. 2009;481:35.
38. Korotcenkov G, Cho BK, Boris I, Han SH, Lychkovsky Y, Karkotsky G. Indium oxide ceramics doped by selenium for one-electrode gas sensors. Sens Actu B. 2012;174:586.
39. Yan YG, Zhang Y, Zeng HB, Zhang LD. In_2O_3 nanotowers: controlled synthesis and mechanism analysis. Cryst Grow Des. 2007;7:940.
40. Ahsanulhaq Q, Maghraby EME, Toshinari Y, Toshio K. Catalyst-free shape controlled synthesis of In2O3 pyramids and octahedron: structural properties and growth mechanism. J Allo Comp. 2009;480:L9.
41. Wang B, Yang YH, Wang CX, Yang GW. Nanostructures and self-catalyzed growth of SnO_2. J Appl Phys. 2005;98:073520.
42. Yan YG, Wang X, Chen HX, Zhou LX, Cao XH, Zhang J. Synthesis of ZnO nanotowers controlled by a reagent's vapour pressure. J Phys D Appl Phys. 2013;46:155304.
43. Neri G, Bonavita A, Rizzo G, Galvagno S, Capone S, Siciliano P. Methanol gas-sensing properties of CeO_2-Fe_2O_3 thin films. Sens Actu B. 2006;114:687.
44. Gonzalez-Vidal JL, Olvera MDL, Maldonado A, Barranca AR, Melendez-Lira M. CO sensitivity of undoped -ZnO, Cr-ZnO and Cu-ZnO thin films obtained by spray pyrolysis. Rev Mexi De Fisi S. 2006;52:6.
45. Park YK, Kim SS. Formation of networked ZnO nanowires by vapor phase growth and their sensing properties with respect to CO. Mate Lett. 2011;65:2755.